Journal of Hydrospace Technology, Vol. 2, No. 2, 1996, pp.14-23

The Effects of Mean-Line Shape on Longitudinal Stability of a Wing in Ground Effect

Wu-Joan Kim * and Myung-Soo Shin †

Abstract

The Reynolds-averaged Navier-Stokes equations for turbulent flow around a two-dimensional foil section moving over a flat surface (roller plate) is solved. The numerical method utilized the finite-difference schemes in collocated grids and the Baldwin-Lomax model is employed for turbulence closure. Calculations are carried out for three foil sections of different mean-line shape with various height ratio. As a foil approaches the bottom surface, the lift is augmented, while there exist some differences in pitching moment due to mean-line shape. It was found that the S-shaped mean line deteriorates lift characteristics but increases pitching moment to restore the designed height.

1 Introduction

Recently Wing-In-Ground effect ship(WIG) draws much attention again as a possible over-seas transportation. The ground effect can be characterized by the augmentation of lift when the airplane approaches the sea surface. The WIG usually has higher lift-drag ratio than the conventional airplane and can be operated comfortably and safely by utilizing the ground effect. The WIG can fill the gap between the traditional ship with low speed and the airplane with high cost, if it is possible to manufacture a large WIG for a liner-type vehicle. The WIG does not require long runaways and can be used as an amphibious vehicle to transport passengers and cargo rapidly in the coastal area and to rescue people in disasters on the sea.

Russia, Japan, China, and Germany paid an effort to develop WIG, especially Russia succeeded to build a very big and fast Ekranoplan(KM) for the military purpose[1]. A research group in St. Petersburg Marine Technical Univ. developed a series of the DHMTU sections with S-shaped mean line to improve the longitudinal stability of WIG[2]. In Korea several researchers studied the feasibility of developing WIG. Kim et al.[3] carried out wind tunnel tests with various foil sections and they made a small flight model to perform free-running test. There have been many numerical studies for wings in ground effects, most of which are based on the potential theory. Recently Hirata and Kodama[4] presented a turbulent flow calculation for a small aspect ratio

*Member, Korea Research Institute of Ships and Ocean Engineering
†Member, Korea Research Institute of Ships and Ocean Engineering

wing with end plates using a multi-block technique. Park et al.[5] tried to perform a numerical study to solve the flow around a whole WIG.

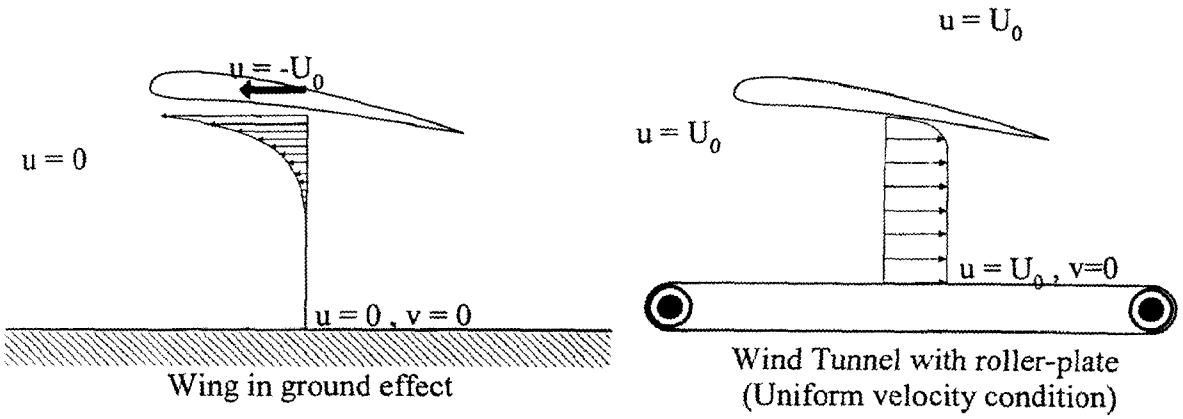

Figure 1 A wing-in-ground effect and computational condition

Traditional airplane wing sections have been tested in the wind tunnel. In this case the foil section is located far from the wind tunnel wall. But the WIG section should be set close to the wall where the viscous boundary layer on tunnel walls will interact with flow near the model, as seen from the computational results of Hirata and Kodama[4]. To avoid such a discrepancy, the roller plate should be installed in the wind tunnel as shown in figure 1. In the followings, numerical methods developed for solving the Reynolds-averaged Navier-Stokes equations and calculated results are presented. Then, first, turbulent flows around a NACA 6409 section with an attack angle 4° are solved for the height ratio of 0.03 - 0.8 to investigate the flow field around a wing near the ground. Next, in order to see the characteristics of S-shaped mean line, NACA 0009 section has been modified with the "sine" mean line of 1% maximum and minimum camber at 25% and 75% chord, respectively. Flows around an original NACA 0009 section and the modified one are also solved to see the variation of pitching moment and center of pressure.

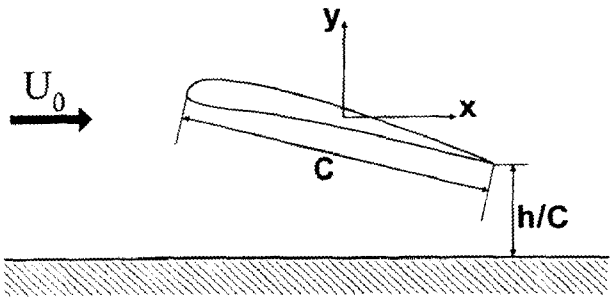

Figure 2 The coordinate system

2 Numerical Methods

2.1 Governing equations

The governing equations for steady turbulent flows in two-dimensional Cartesian coordinates, i.e., the Reynolds-averaged Navier-Stokes equations and the continuity equation can be written as follows. As shown in figure 2, x denotes the downstream direction and y is in the opposite direction to the gravity. (u, v) means the velocity components in (x, y) direction, respectively, and the coordinate origin is located at the mid-chord point.

Continuity equation

$$\frac{\partial u_k}{\partial x_k} = 0 \tag{1}$$

Momentum transport equations

$$\frac{\partial u_i}{\partial t} + u_j \frac{\partial u_i}{\partial x_j} = -\frac{\partial p}{\partial x_i} + \frac{1}{R_{eff}} \nabla^2 u_i + \frac{\partial \nu_t}{\partial x_j} \left(\frac{\partial u_j}{\partial x_i} + \frac{\partial u_i}{\partial x_j} \right) \tag{2}$$

where, $\frac{1}{R_{eff}} = \frac{1}{Re} + \nu_t$ and the summation convention is applied over repeated indices. The chord length C, the fluid density ρ and incoming flow velocity U_o are utilized for non-dimensionalization. Reynolds number is defined as $Re = \frac{U_o C}{\nu}$,where ν is the kinematic viscosity of the air. The eddy viscosity ν_t is determined by using Baldwin-Lomax turbulence model. To apply the finite difference schemes easily, the above governing equations are transformed into generalized curvilinear coordinates and the resulting equations are given in the followings.

Continuity equation

$$\frac{1}{J} \frac{\partial}{\partial \xi^m} (J U^m) = \frac{1}{J} \frac{\partial}{\partial \xi^m} (b_i^m u_i) = 0 \tag{3}$$

Momentum transport equations

$$\frac{\partial u_i}{\partial t} + U^k \frac{\partial u_i}{\partial \xi^k} = -\frac{1}{J} b_i^k \frac{\partial p}{\partial \xi^k} + \frac{1}{R_{eff}} \nabla^2 u_i + \left(\frac{1}{J} b_j^k \frac{\partial \nu_t}{\partial \xi^k} \right) \left[\left(\frac{1}{J} b_i^m \frac{\partial u_j}{\partial \xi^m} \right) + \left(\frac{1}{J} b_j^m \frac{\partial u_i}{\partial \xi^m} \right) \right] \tag{4}$$

Here, the contravariant velocity components are defined by $U^k = \frac{1}{J} b_j^k u_j$, and other geometry-related coefficients can be found in Kim[6,7].

2.2 Discretization and velocity-pressure coupling

Transformed momentum transport equations are integrated in time using the Euler-Implicit method and the third order upwind-biased scheme is used for the convection terms, while the second order central difference scheme is applied for the diffusion terms. Discretized linear equations are solved by using ADI(Alternate-Direction-Implicit) , for which one can use a vectorized penta-diagonal solver. The pressure field is obtained by

solving pressure-Poisson equation using the similar method to the MAC-type projection method. In the present study, since non-staggered grid system is adopted, the fourth order dissipation term is added in the Poisson equation to avoid oscillation in pressure field (Checker-board problem).

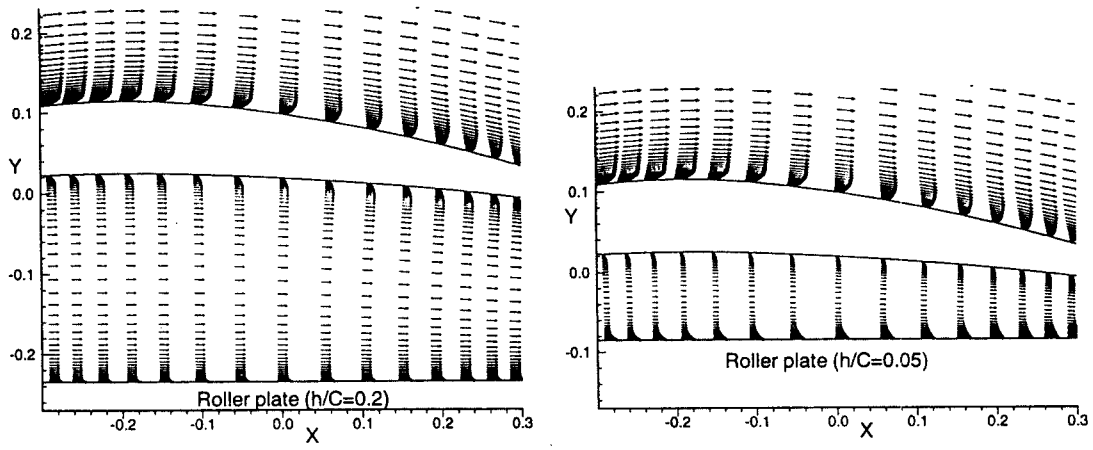

Figure 3 Velocity vectors around NACA 6409 section at h/C=0.05, 0.2 ($\alpha = 4^o$)

2.3 Boundary conditions and solution procedure

In the present study, two-block H-grid topology is adopted for above and below the foil surface and two grid points from each block is overlapped to insure the continuity of flow field. No-slip condition is applied to the foil surface, while a uniform flow condition depicting a roller plate is applied for the flat bottom surface. Free stream condition is applied at the outer surface far from the foil and uniform flow is given at upstream boundary, while the velocity is extrapolated at the downstream boundary.

First of all, the grid system is generated using elliptic partial differential equations. Knight's method[8] is utilized to solve the Poisson equation. It was chosen for its simplicity since control functions can be automatically determined based on given boundary points. With the grid system obtained by the solution of Poisson equation, geometry-related terms are calculated. Then, the linearized momentum transport equations are solved with a presumed pressure field using ADI scheme. With new velocity components, the pressure field in the next time step is obtained by solving pressure-Poisson equation. Iteration gives the final converged solution.

3 Results and discussion

The coordinate system used for the calculation and presentation of the results is shown in figure 2.

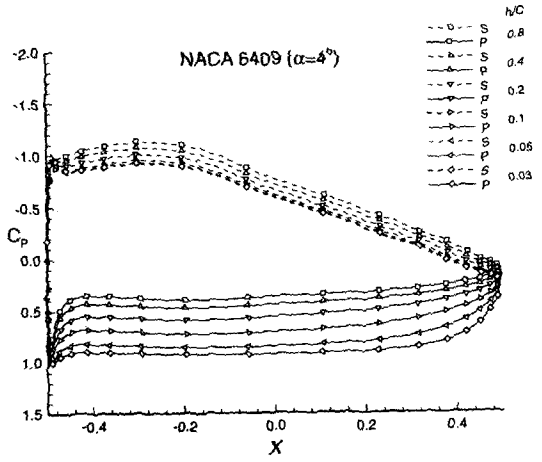

Figure 4 Pressure distribution on NACA 6409 section with $\alpha = 4^o$ (h/C=0.03-0.8)

The origin is located at the mid-chord point of the foil, and the length is non-dimensionalized by using the chord length C. Reynolds number for the calculation was $Re = 2.37X10^5$, similar to the case of Kim et al.[3] and the angle of attack was fixed at 4^o. 150X120 grids were used to simulate turbulent flow, 300 - 500 seconds were required to get a converged solution on the CRAY C-90. First, the flow around a NACA 6409 section is explored to investigate the ground effect. Next, the flow around a NACA 0009 section and modified one with "sine" mean line are studied to see the effect of S-shaped mean line on the pitching moment.

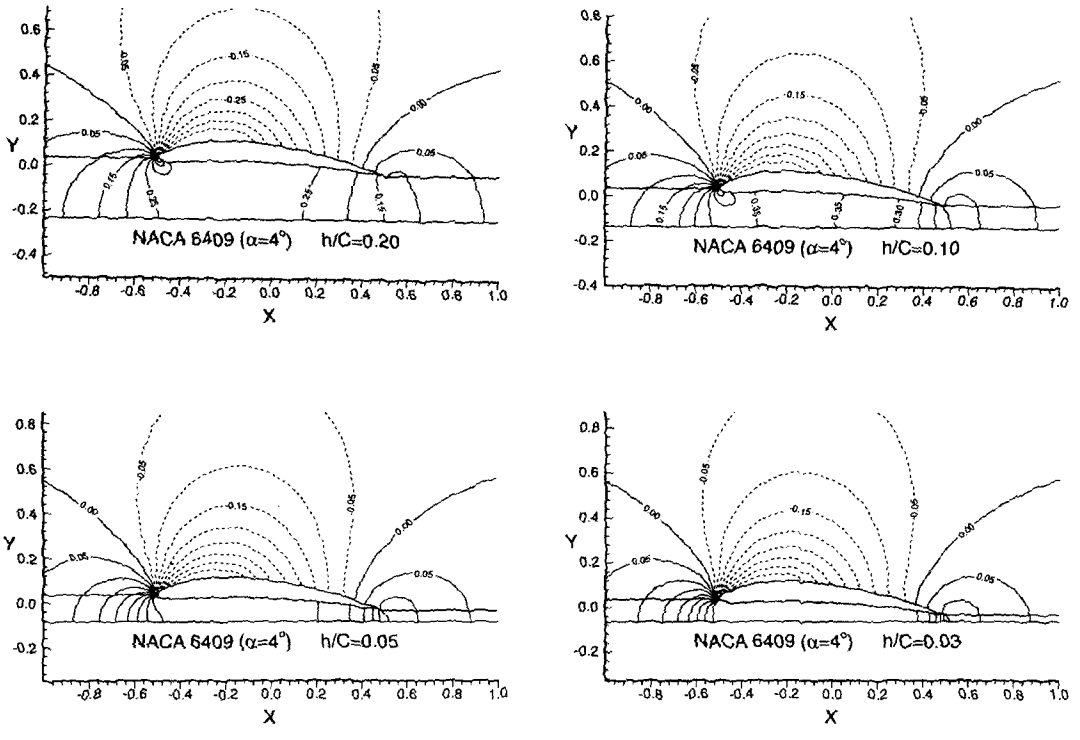

Figure 5 Pressure contours around NACA 6409 section ($\alpha = 4^o$)

In figure 3 flow vectors above and below the NACA 6409 section is shown for h/C=0.05 and 0.2. It is observed that the magnitude of velocity becomes quite different as the foil gets closer to the bottom surface, since the flow below the foil section is retarded and locked in. This results in the high pressure region beneath the foil which contributes to the lift increase. The foil surface pressure distributions are shown in figure 4. As the foil approaches the bottom surface, the pressure on the lower surface(pressure side) increases , its distribution becomes flatter, and high pressure near the trailing edge contribute to the decrease of the pitching moment, since the pitching moment was defined as positive nose up with respect to the mid-chord point. Figure 5 shows pressure contours around the NACA 6409 with various height ratio. As noted earlier, the main feature of pressure contours is the increase of pressure on the lower surface of the foil(pressure side).

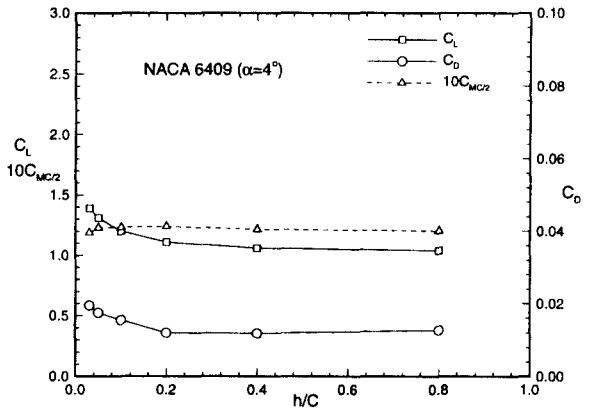

Figure 6 Lift, drag, and pitching moment coefficients of NACA 6409 section

Integrated lift, drag, and pitching moment are shown in figure 6. As the foil section approaches the bottom surface, lift increases. But drag also increases due to high pressure region on the lower side with downward slope, which limits the increase of lift-drag ratio. Figure 7 shows the change of stagnation (flow attachment) point due to the variation of height ratio. We see that the local flow angle becomes larger as h/C decreases. However, for NACA6409 section, the pitching moment decreases a little. This fact implies that the center of pressure moves backward as h/C decreases. The center of pressure is located at 38.4% from the leading edge when h/C=0.8, at 39.7% when h/C=0.1, and at 41.5% when h/C=0.03. This backward shift of center of pressure mainly destabilizes the WIG, since the decrease of pitching moment reduces the effective attack angle. And this in turn results in lift reduction, which makes the WIG approache the bottom surface more. Thus, NACA 6409 section provides reasonably large lift-drag ratio, but may generate a serious problem of longitudinal stability.

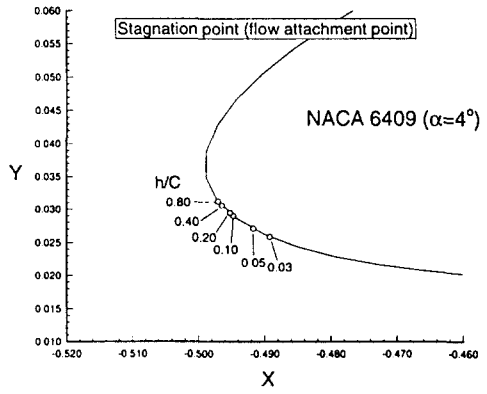

Figure 7 Flow attachment points near leading edge at h/C=0.03-0.8

Russian-developed DHMTU section is known to have S-shaped mean line for the longitudinal stability. In order to see the effect of S-shaped mean line, two sections were selected. NACA 0009 section is chosen to be a basic section, since it has zero camber. Then, the mean line of NACA 0009 section is modified by $0.01sin(2\pi x)$, which exaggerate the effect of S-shape mean line. Modified NACA 0009 section has the "sine" mean line of 1% maximum and minimum camber at 25% and 75% chord, respectively. Figure 8 shows the shape of selected foil sections, where dashed line denotes to the original NACA 0009 section, while solid line represents modified one. The pressure distribution on two sections at the attack angle of $2^o, 4^o, 6^o$ in an unbounded fluid is shown in figure 9 and 10. The main feature of modified NACA 0009 section is the reversal of pressure coefficient occurring at the 40% chord ahead of the trailing edge. This reversal increases the pitching moment and moves the center of pressure toward the leading edge, compared to the original NACA 0009 section. However, the resulting lift is smaller, since the loss of lift component occurs after the pressure reversal. The pressure distributions of NACA 0009 section and modified one with the attack angle 4^o at various height ratio are shown in figure 11 and 12. Increase of pressure on the lower surface of the foil is not very prominent compared to the previous NACA 6409 section, and the so-called "Venturi effect" occurs when the foil is very close to the bottom surface due to the convex curvature of the lower surface of the foil. This phenomenon is severer for modified NACA 0009 section due to the S-shape mean line.

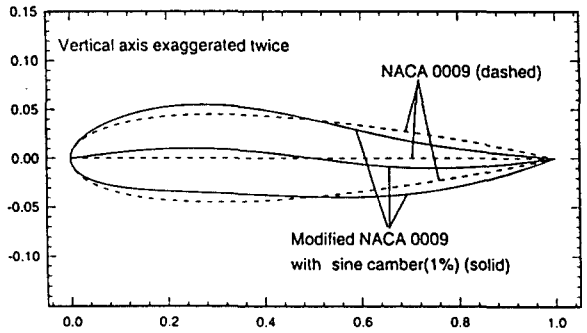

Figure 8 Section profiles of original and modified NACA 0009 section

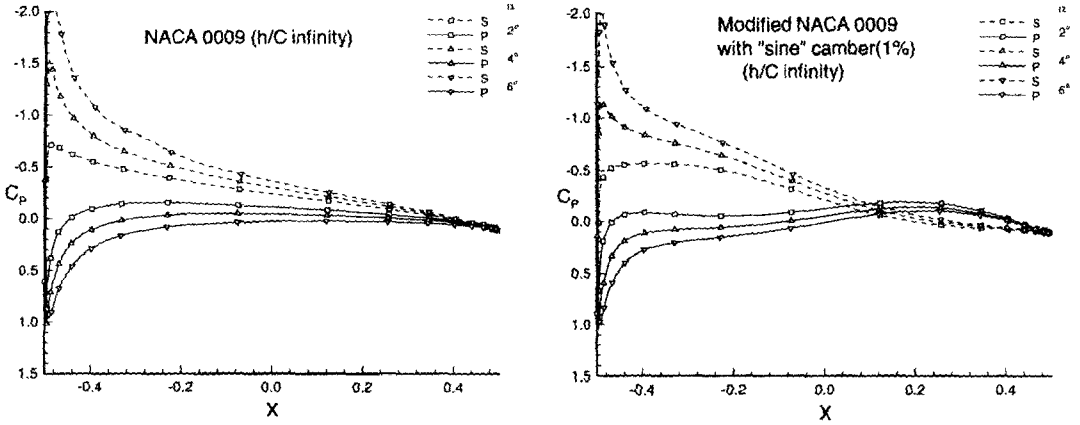

Figure 9 Pressure distribution on original and modified NACA 0009 section

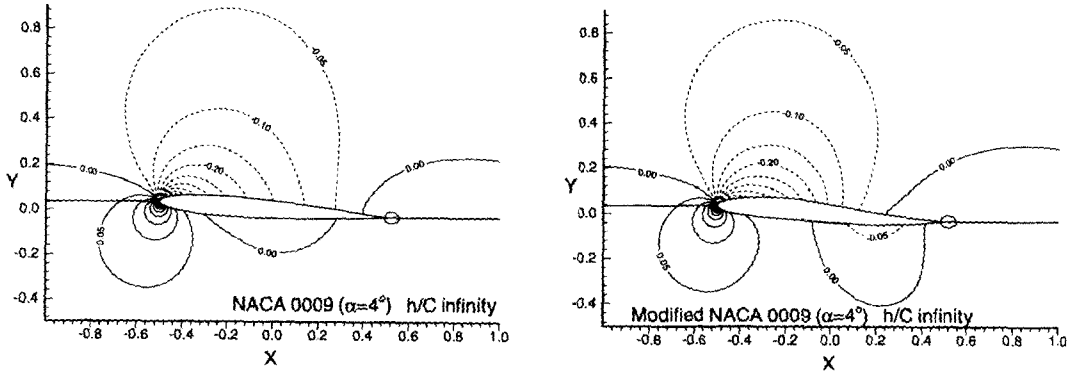

Figure 10 Pressure contours around original and modified NACA 0009 section

Figure 13 shows the comparison of lift, drag, and pitching moment for two sections. Increase of lift is not very big for both cases, but that of pitching moment is. The center of pressure of the original NACA 0009 section is located at 24.2% from the leading edge in an unbounded fluid, at 25.5% for h/C=0.4, at 23.9% for h/C=0.1, and 19.0% for h/C=0.03. The center of pressure moves slightly (about 5%) forward as NACA 0009 approaches the bottom surface. For the modified NACA 0009 with "sine" mean line, the center of pressure is at 14.8% from the leading edge in unbounded fluid, at 16.5% for h/C=0.4, at 15.0% for h/C=0.1, and at 6.4% for h/C=0.03. The center of pressure moves forward much (about 9%), as the foil approaches the bottom surface. It should be mentioned at this point that the present cases are chosen to exaggerate the phenomenon. As noted earlier, the forward movement of the center of pressure and the increase of pitching moment will stabilizes the WIG, since the increment o pitching moment will result in the increase of effective attack angle hence the lift, so a to make it restored to the original position. However, the severe increment of pitchin moment due to the section change will deteriorate the gain by using WIG, thus, tl designer should compromise between the high lift-drag ratio with concave curvatu and the increment of pitching moment with convex curvature of the lower surface ahe of trailing edge.

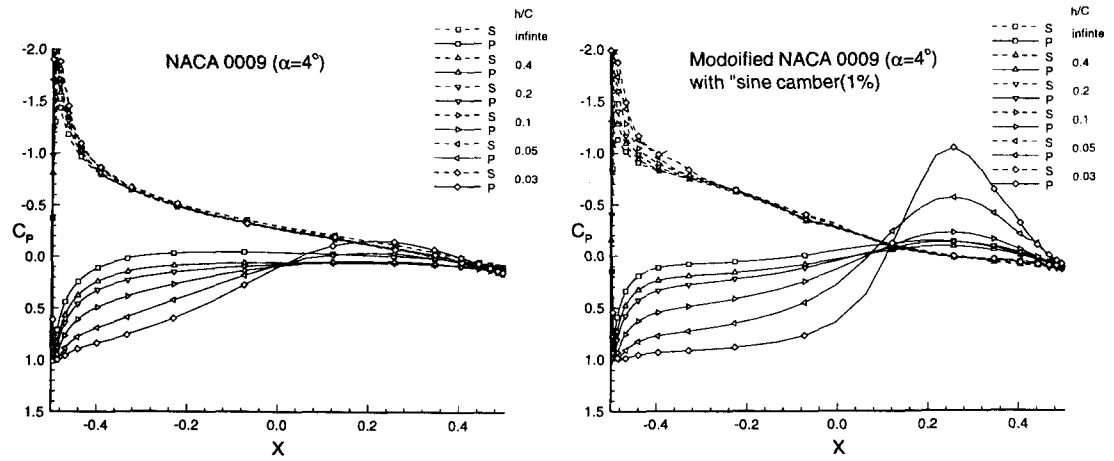

Figure 11 Pressure distribution on original and modified NACA 0009 section ($\alpha = 4^o$)

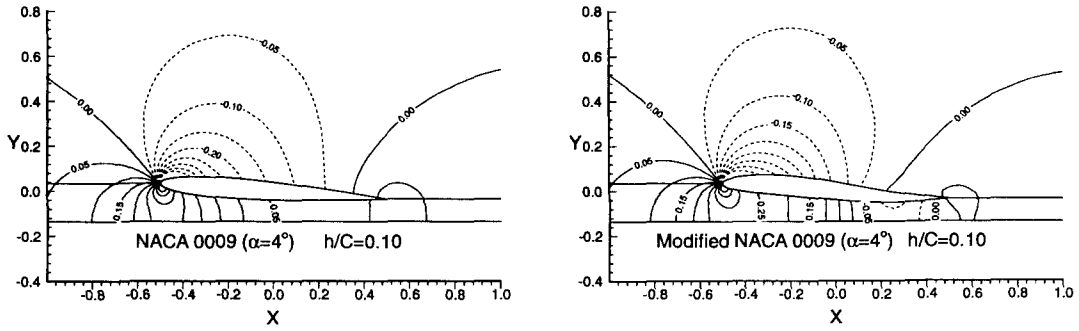

Figure 12 Pressure contours around original and modified NACA 0009 section at h/C = 0.1 ($\alpha = 4^o$)

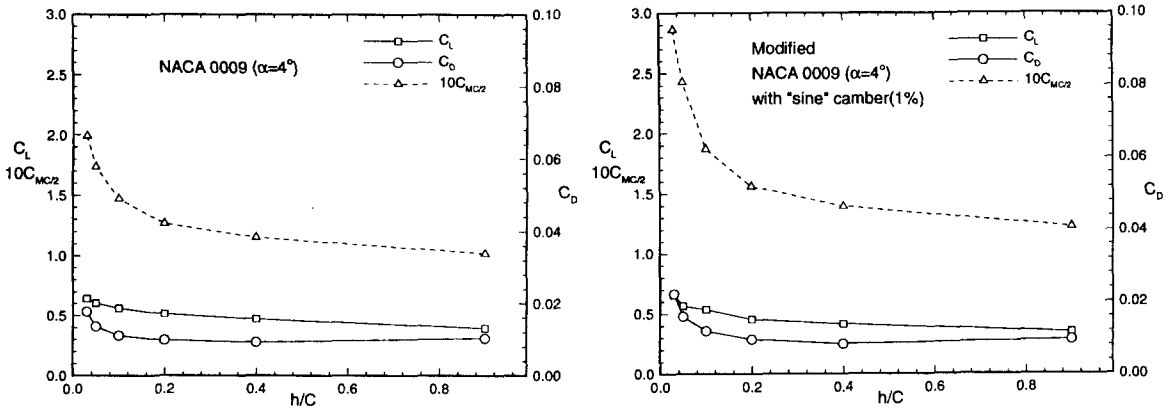

Figure 13 Lift, drag, and pitching moment coefficients of original and modified NACA 0009 section

4 Concluding remarks

Turbulent flows around three foil sections moving over a roller plate are calculated to see the ground effect and the influence of mean line shape. The Reynolds-averaged Navier-Stokes equations are solved with Baldwind-Lomax turbulent model for NACA 6409, NACA 0009, and modified NACA 0009 with "sine" mean line at the angle of attack of 4^o. The bottom boundary condition implies that the roller plate moves at the same speed as incoming flow, which simulates the WIG moves over the no-slip surface.

The calculated results for NACA 6409 section shows that as the foil approaches the bottom surface, the lift is augmented, while the center of pressure moves backward slightly, and the pitching moment decreases. The lift increment is mainly due to the fact that the pressure on the lower surface becomes higher and nearly constant. The comparison of NACA 0009 section and the modified one shows that there exist some differences in pitching moment due to mean-line shape. It was found that the S-shaped mean line deteriorates lift characteristics but increases pitching moment to regain the designed height.

Acknowledgement

This paper is based on the results of the project "the development of passenger WIG ship (GN183)", supported by the Ministry of Science and Technology of Korea.

References

[1] Rozhdeskvensky, K.V. (1995), " State-of-the-art of Russian R & D on Ekranoplans," *Workshop on Wing-in Ground Effect Ship Technology,* KRISO.

[2] Kornev, N.V. (1995), "Problems of stability in Ekranoplans," *Workshop on Wing-in-Ground Effect Ship Technology,* KRISO.

[3] Kim, S.K., Kim, J.H., Suh, S.B. (1995), "Wind tunnel experiment of WIG sections," *Proceedings of Fall Meeting of Society of Naval Architecture of Korea.*

[4] Hirata, N., Kodama, Y. (1995), "Flow computation for three-dimensional wing in ground effect using multi-block technique," *Journal of The Society of Naval Architecture of Japan,* Vol. 177.

[5] Park, J.C., Shin, M.S., Yang,.S.I. (1995), "Numerical calculation of flow around a WIG," *Proceedings of Fall Meeting of Society of Naval Architecture of Korea,* 1995.

[6] Kim, W.J., Van, S.H., Hyun, B.S. (1994), Study on the pressure distribution around a hydrofoil near the free surface, *KRISO Report UCE554-1845D.*

[7] Kim, W.J., Van, S.H. (1995) "An experimental and computational study on the flow around a hydrofoil with a free surface," *Journal of Hydrospace Technology,* Vol. 1, No. 2.

[8] Visbal, M., Knight, D. (1982), "Generation of orthogonal and nearly orthogonal coordinates with grid control near boundaries," *AIAA Journal,* Vol. 20, No. 3.